

Evidence of Negative Heat Capacity, Rigidity Percolation and Intermediate Phase in Fast Ion Conducting Conditional Glasses

B. Tanujit and S. Asokan^{a)}

Department of Instrumentation and Applied Physics
Indian Institute of Science, Bangalore – 560 012, India

Abstract

In this work, we report the rigidity percolation phenomena in a fast ion conducting (FIC), conditional glass forming system, $(\text{AgI})_{75-x}(\text{Ag}_2\text{O})-(\text{MoO}_3)_x$. In the pursuit of where and why the rigidity percolation thresholds appear within the glass forming range of $20 \leq x \leq 37.5$, calorimetry and photoelectron spectroscopy experiments have been performed. It is found that the temperature dependence of normalized, in-phase heat capacity, at glass transition temperature, exhibits more fluctuations for samples with higher AgI concentration. This suggests a fragility threshold within the composition range, since the fluctuations indicate a non-Arrhenius type relaxation behavior related to fragile glass. Furthermore, we observe a sign shift in the measured, in-phase heat capacity value that reveals the fragility threshold. The negative heat capacity in the non-Arrhenius region has been corroborated with the thermodynamic behavior of nanoclusters. The negative heat capacity and presence of nanoclusters have been used and discussed to provide evidence for a nanoscale phase separation. The photoelectron spectroscopy study shows the formation of essential covalent structural units, $[-\text{Mo}-\text{O}-\text{Ag}-\text{O}-]$ and complex molybdenum oxides in the Arrhenius type rigid region. Finally, the non-reversing enthalpy profile has been studied over the whole composition range. The global, square well minima sandwiched between floppy and stress rigid phase has been found to denote the intermediate phase, in the range $32.25 \leq x \leq 35$.

^{a)} Corresponding Author email: sundarrajan.asokan@gmail.com, sasokan@iisc.ac.in

Kauzmann's glass condition states that $\partial(H_{\text{liquid}} - H_{\text{crystal}})/\partial T$ drops to zero during glass transformation [1] where H denotes the enthalpy of the indexed state and T is the temperature; in other words, across the glass transition temperature (T_g), the configurational entropy (S_c) remains continuous during liquid to solid transition [1], at T_g , $\Delta S_c = (S_{c\text{ liquid}} - S_{c\text{ solid}}) = 0$ [2]. To microscopically realize this phenomena, J. Phillips and M. Thorpe [2-5] introduced a site-bond type mechanical constraints model, for systems that constitute covalent bonds, dominantly. This formalism considers only the nearest-neighbor, central, two-body bond-stretching and non-central, three body bond-bending forces. The model, when associated with the glass condition $\Delta S_c = 0$, incorporating average first coordination number and medium range order, the entropic glass condition, convolutes into a constraints equation $N_{\text{Con}} = N_d$, where N_{Con} is the number of interatomic force field constraints per atom and N_d is the number of vector degrees of freedom per atom [2, 5]. In a covalent network structure, the constraints condition acts like a rigidity percolation threshold. The condition $N_{\text{Con}} < N_d$ refers to a floppy (FP), polymeric phase, e.g. a linear network in three dimension $N_{\text{Con}} = 2$ and $N_d = 3$. As more constraints get accommodated within the system, with compositional variation, the interconnectivity among the sites increases and rigidity percolates through the system; this phase is known as stressed rigid amorphous phase (SRP) when $N_{\text{Con}} > N_d$ [5].

Contemporaneous study on the phenomena of photo-melting in As_2S_3 glass [6] and giant photo-contraction in obliquely deposited porous GeSe_2 [7] could relate to another stable phase where the network is mechanically rigid but stress free [8]. This 'trapped in limbo' phase in rigidity transition corresponds to $N_{\text{Con}} = N_d \Rightarrow \Delta S_c = 0$ [9]. Boolchand et al. [8-11] rigorously investigated and identified this stress-free phase as an Intermediate Phase (IP) that appears in between the FP and SRP. IP glasses exhibit a non-aging behavior, an optimal glass forming tendency [12] and they possess a self-organization functionality [9] which is the global reconnection of chemical bonds to form stress-free networks [12]. This functionality along with the constraints model has been used to understand protein folding and protein phase transition [13]. The self-organization and IP have been recognized in thin-film transistor used in liquid crystal display [14]; and further exploited in various disciplines e.g. Soft condensed matter, Computer science, Electrical engineering, Protein science etc. [12, 14].

Early studies on rigidity transition and IP [8-11] have been conducted on chalcogen (S, Se, Te) based glasses which exhibit a continuous covalent random network (CRN) topology that is essential for rigidity transition. Oxygen, having a high electronegativity and a tendency to form O^- and O^{2-} , differs significantly from other chalcogens [15] in terms of network topology and chemical properties. When network modifier is introduced into a base oxide glass, non-bridging oxygen (NBO) forms and ionically

bonds with modifier cation; these phenomena alters the network topology [15]. Interestingly, three phased rigidity transition has been observed in oxide glasses, such as AgI based FIC glasses e.g. $(\text{AgI})_x(\text{AgPO}_3)_{1-x}$ [16-17], $(\text{Na}_2\text{O})_x(\text{GeO}_2)_{1-x}$ [18] and $(\text{Na}_2\text{O})_x(\text{SiO}_2)_{1-x}$ [19]. However, the constituent glass forming agents for these glasses are P_2O_5 , GeO_2 and SiO_2 respectively, all of which are strongly covalent glass formers [20-21] and follow Zachariasen's rules for glass formation as CRN [20].

Upon increasing the modifier oxide concentration within the base glass environment, the depolymerization of CRN occurs by bridging oxygen (BO) to NBO conversion and formation of Q_n species, where $Q_n = [\text{AO}_{\frac{n}{2}}\text{O}_m]^{m-}$, ($n + m \leq 4$ and $A = \text{P, Ge, Si}$) and there is a gradual change from ultra to ortho [20]. However, heavy transition metals e.g. Mo, W capable of existing in multiple valance states; are 'conditional' oxide glass formers [20]. Pure liquids of these transition metal oxide compounds essentially require modifier or another network forming oxide for glass formation, BO to NBO conversion, different Q_n species and modifier cation formation. The ionic character of these metallic elements and ionic bonding or 'partial covalence' [22-23] between modifier cations and NBOs, significantly enhance the non-covalent, non-directional bonding nature of these type of glassy systems. These bonds disconnect the covalent graph and form fragile molecular solid where interatomic strong and intermolecular weak force coexist [15].

Besides, in the viscosity-temperature profile, liquids that deviate slightly from Arrhenius type behavior, exhibit small changes in heat capacity at T_g ; this change is large for fragile glasses with a lack of directional bonds [24] i.e. non-directionality of bond enhances the non-Arrhenius type behavior in the profile. The structural disparity, in terms of the origin of First Sharp Diffraction Peak (FSDP), between these two types of glasses, has been reported and discussed by Swenson et al. [25]. In case of molecular (oxide) glasses, FSDP is significantly contributed by oxygen which is in contrary with other glass formers, e.g. phosphate [26] and borate [27] glasses. Thus, these conditional glass formers, transition metal oxides are significantly different, in a chemical and topological sense, from CRN forming Chalcogenide and metalloid/non-metal oxides.

In this present work, we report the rigidity percolation phenomena in $(\text{AgI})_{75-x}(\text{Ag}_2\text{O})_{25}(\text{MoO}_3)_x$ fast ion conducting glassy system, in a broad composition range, $20 \leq x \leq 37.5$, primarily pursuing the questions where, why and how the rigidity transition should occur? In order to answer these questions, Alternating Differential Scanning Calorimetry (ADSC) and X-ray Photoelectron Spectroscopy (XPS) experiments have been conducted.

At first, the fragility behavior from the fluctuating nature of heat capacity in glass transition temperature is studied. The fragile nature of the system transforms rapidly at a composition threshold. The compositional range below this threshold has been identified as Nanoscale phase separation (NSPS) regime. To describe this transformation, we have studied the absolute value of the heat capacity of all the samples. The absolute value of heat capacity shows a change in sign in that threshold i.e. from negative to positive. The thermodynamic meaning of negative heat capacity has been corroborated with the nanostructure of the system.

To summarize, a composition threshold has been identified below which the glassy system exhibits NSPS. This threshold segregates two regions based on the nature of bonding; the NSPS consists of non-directional, long range ionic bonds that gradually get replaced by the covalent bonds beyond the threshold with increasing MoO_3 concentration. The XPS study recognizes the bond as $[-\text{Mo}-\text{O}-\text{Ag}-\text{O}_\text{L}-]$ and complex molybdenum oxide. Finally, the non-reversing enthalpy (ΔH_{nr}) value exhibits a global minima which is the IP, sandwiched between under-constrained FP and over-constrained SRP. Our observations establish the rigidity percolation in an ion conducting conditional glass forming system and it proposes a novel method to find the fragility threshold and NSPS.

$(\text{AgI})_{75-x}-(\text{Ag}_2\text{O})_{25}-(\text{MoO}_3)_x$ solid electrolyte glasses, in the composition range, $20 \leq x \leq 37.5$, have been synthesized, by thoroughly mixing constituent compounds as a fine homogeneous powder, and melting it in a 2450 MHz-900 watts microwave oven for 10-12 minutes and subsequently quenching the melt, down to room temperature between two steel plates. The idea of keeping Ag_2O concentration constant while varying AgI and MoO_3 concentration, along with the novelty of using microwave heating technique has been discussed in detail elsewhere. [28]

ADSC studies are carried out using a Mettler Toledo 822e ADSC instrument operated at $3^\circ\text{C}/\text{min}$ scan rate with 1°C scan amplitude, in the temperature range 40°C to 200°C for ‘as quenched’ samples (~ 15 mg) of approximately equal thickness. The obtained heat flow and heat capacity data have been analyzed using the STAR[®] and OriginPro software. The XPS study has been carried out in an AXIS Ultra XPS instrument with monochromatic Al X-ray source. The binding energy scale has been calibrated with C1s 284.8 eV peak. The obtained data are fitted with Gaussian-Lorentzian peak profile after U2 Tougaard background subtraction with Casa XPS software.

The change in configurational entropy during liquid to solid transition $\Delta S_c = (S_{c\text{ liquid}} - S_{c\text{ solid}})$ is directly related to two measurable quantities, ΔH_{nr} and T_g by the form of $\Delta S_c = \Delta H_{\text{nr}}/T_g$ [12]. When the model solid is glass, $\Delta S_c = 0$, which indicates that the configurational freedom of glass and liquid are the

same, otherwise $\Delta S_c > 0$. Apparently, this feature of configurational entropy is directly reflected upon ΔH_{nr} . In the ADSC experiment, the non-reversing heat flow signal exhibits a Gaussian profile encompassing T_g , the area under that profile yields ΔH_{nr} [17]. Furthermore, as ADSC involves a sinusoidal modulated heat flow response, the resultant heat flow gets associated with a non-zero phase lag (ϕ). And hence, the total heat capacity (C^*) is represented by using complex notation, the real, in-phase, phase corrected reversing heat capacity ($C_{pPCR} = C^* \cdot \cos\phi$) and out-of-phase, kinetic heat capacity ($C_{pK} = C^* \cdot \sin\phi$). Other than melting, this phase correction of heat capacity is negligible i.e. $C^* \approx C_{pPCR}$ [29]. Thus measuring in-phase heat capacity along with ΔH_{nr} has played very important role from two different perspectives.

A large fluctuation in heat capacity near T_g is a manifestation of deviation from an Arrhenius type relaxation behavior due to increase in non-directional bonds; whereas significant amount of directional covalent bonds form a strong system [30, 31] which is a necessary requirement for rigidity transition. A non-Arrhenius type behavior suggests the system's high vulnerability towards thermal and structural degradation. Thus, determining the fragile and strong compositions for the present glass has a significant importance in the context of rigidity transition, fragility and relaxation.

Figure-1(a) shows the phase corrected, in-phase heat capacity, represented as C_{pPCR} , (normalized to the range [0, 1]) versus T/T_g plot for two different representative samples, $(AgI)_{50}-(Ag_2O)_{25}-(MoO_3)_{25}$ and $(AgI)_{42.25}-(Ag_2O)_{25}-(MoO_3)_{32.75}$. Clearly, near T_g , glass with higher AgI concentration i.e. $(AgI)_{50}-(Ag_2O)_{25}-(MoO_3)_{25}$ exhibits more fluctuations in $C_{pPCR}-T/T_g$ profile than the other, indicating a fragile nature and deviation from Arrhenius type relaxation in viscosity. The role of AgI is to expand the free volume to enhance the ionic conductivity [32]. The present result corroborates with this understanding of the role of AgI. The expansion in the glass matrix causes creation of free volume and lower coordination that directly impact the $C_{pPCR}-T/T_g$ profile; with higher AgI concentration, the glass system becomes more fragile.

It is interesting to explore how this fluctuating $C_{pPCR}-T/T_g$ profile gets stabilized or how the fragile-strong transition occurs over compositions. Interestingly, there is a threshold where the nature of fluctuation changes abruptly, indicating a transition from a fragile to a strong system. The abrupt change occurs in the sign of the measured or absolute (not normalized) value of C_{pPCR} . As the sign of C_{pPCR} for an individual sample remains same over the ADSC scanning range (40°C-200°C), C_{pPCR} at T_g i.e. $C_{pPCR}(T_g)$ is considered as an indicator of the sign of C_{pPCR} .

Figure-1(b) shows $C_{pPCR}(T_g)$ values for all the compositions along with T_g . The T_g increases monotonically with the increase in MoO_3 concentration. However, $C_{pPCR}(T_g)$ shifts from being negative

(Region-I) to positive (Region-II) almost abruptly at a threshold between $(\text{AgI})_{30}-(\text{Ag}_2\text{O})_{25}-(\text{MoO}_3)_{45}$ and $(\text{AgI})_{31.25}-(\text{Ag}_2\text{O})_{25}-(\text{MoO}_3)_{43.75}$. This shift in $C_{\text{pPCR}}(T_g)$ profile indicates a very important aspect of the structure of the sample. Besides, samples with negative $C_{\text{pPCR}}(T_g)$ value, exhibit more fluctuations in normalized $C_{\text{pPCR}}-T/T_g$ profile than the samples with positive $C_{\text{pPCR}}(T_g)$ value.

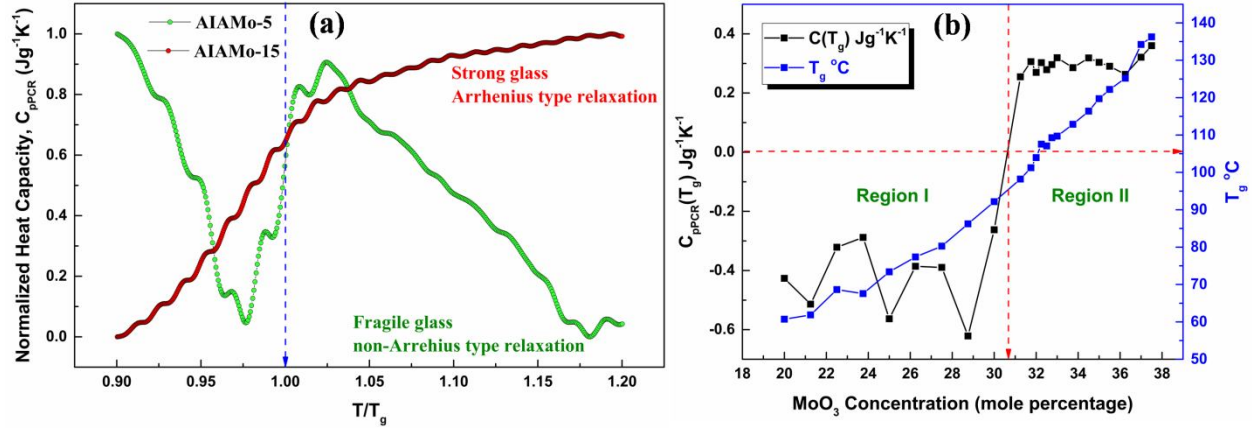


Figure-1:(a) C_{pPCR} (Jg⁻¹K⁻¹) (normalized to the range [0, 1]) versus T/T_g plot for two representative samples, $(\text{AgI})_{50}-(\text{Ag}_2\text{O})_{25}-(\text{MoO}_3)_{25}$ and $(\text{AgI})_{42.25}-(\text{Ag}_2\text{O})_{25}-(\text{MoO}_3)_{32.75}$. (b) Measured (not normalized) values of $C_{\text{pPCR}}(T_g)$ (Jg⁻¹K⁻¹) and T_g °C vs. MoO₃ concentration (mole percentage).

This scenario needs to be considered from two perspectives; what does negative C_{pPCR} mean exclusively for this sample and thermodynamically. In an important study on the effect of pressure on conductivity in AgI-Ag₂O-MoO₃ glassy system by H Senapati et al. [33] suggested a tissue and cluster type structural model where the whole glass structure is composed of clusters which are connected by less dense and compressible tissue material. Initially, the applied pressure influences the tissue by reorganizing it to yield a structure similar to that of cluster.

The schematic in Figure-2 shows this [33] effect of pressure on the total volume (V_{Total}) that constitutes of tissue and cluster. In other words, with pressure (p), the tissue volume (V_{tissue}) decreases in expense of the increase in cluster volume (V_{cluster}) i.e. in an isothermal process, V_{Total} under pressure remain constant;

$$V_{\text{Total}} = V_{\text{tissue}} + V_{\text{cluster}} = \text{Constant} \quad \dots (1)$$

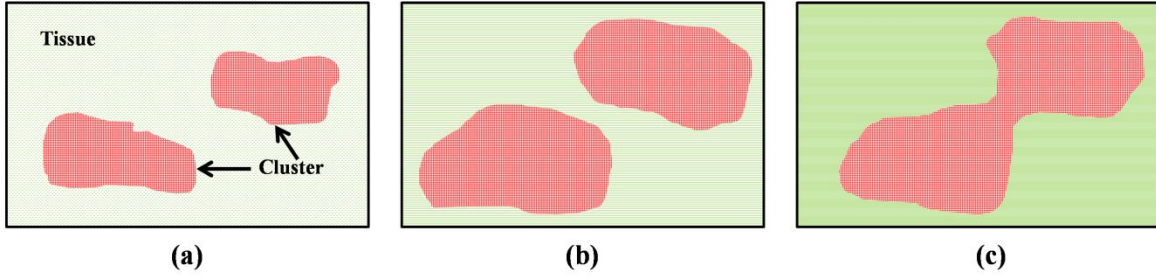


Figure-2:(a) A segment of V_{Total} which is under pressure constitutes of dense cluster and less dense, compressible tissue. (b) As the pressure increases, the tissue reorganizes to yield a structure similar to the cluster. (c) Higher pressure can change tissue region in between two clusters and thus connecting them while increasing the cluster volume. Pressure increases from (a) to (c)

Thus, the thermodynamic quantity,

$$\left(\frac{\partial P}{\partial V}\right)_T = 0 \dots (2)$$

Now the thermodynamic relation,

$$C_p - C_v = -\left(\frac{\partial P}{\partial V}\right)_T T \left(\frac{\partial V}{\partial T}\right)_P^2 \dots (3)$$

Where C_p and C_v are isobaric and isochoric heat capacities respectively, becomes

$$C_p - C_v = 0 \dots (4)$$

Hence the experimentally obtained $C_{p\text{PCR}}$ and the relation (4) substantiate an equal sign for C_v .

Now, in the thermodynamic context, negative C_v is undoubtedly a compelling topic in the branch that concerns thermodynamic behavior of nanoclusters where two different structural phases separated by free energy barrier [34]. Negative $C_v (\equiv (\partial E / \partial T)_V)$ is a consequence of the ‘S’ shaped bend in the caloric curve, which has been argued to be the indication of a dynamic phase coexistence [35-37, 39]. In a critical temperature, small finite system undergoes critical oscillation between two metastable states, giving rise to the negative slope in the caloric curve [34-40].

Thus, incorporating these two assertions, ‘sample based’ and thermodynamic, it is suggested that experimentally obtained negative $C_{p\text{PCR}}$ is a reflection of a structural phase consisted of tissue and cluster discussed earlier. This type of nanoclustering, segregated from backbone forming glass matrix, is the NSPS phenomena. NSPS has been observed earlier in certain glassy systems in some studies on rigidity

transition while their detection of NSPS has been based on structural characterizations e.g. X-ray diffraction, Raman, etc. [8, 12, 16, 41-44]. Within the NSPS region, samples exhibit a non-Arrhenius nature of heat capacity near T_g . The NSPS occurs within the compositional range because of loss of network connectivity. Thus this fragility threshold, defined as the sign shift of C_{pPCR} , can be regarded as a shift from a less connected to a highly connected network. To explain this nature of network connectivity or bonding in terms of chemical states of the constituents, we performed XPS for some of the samples from region-I and region-II.

High resolution XPS peaks for Ag3d, Mo3d and O1s spectrums have been obtained. The binding energy (BE) for Ag3d_{5/2} peak is at 367.3 eV for region-I and 366.8 eV for region-II i.e. $\Delta BE = BE(\text{final}) - BE(\text{initial}) < 0$. Early studies have assigned the 367.3 eV peak to Ag3d_{5/2} peak for Ag₂O where the oxidation state of Ag is +1 and 366.8 eV peak for AgO that contains an equimolar mixture of Ag(+1) and Ag(+3) oxidation states that appear to have an average valency of Ag²⁺ [45,46]. Surface content of silver for the sample mostly gets oxidized, giving rise to only Ag3d_{5/2} peak for Ag-O bond, whilst Ag-I remains very weak, indicating that the features of AgI comes within the bulk property of the sample. The binding energy for Mo3d_{5/2} in the spectrum appears at 230.63 eV and 231.18 eV. This suggests that the oxidation of Mo consisted of Mo⁴⁺ and Mo⁵⁺ species respectively [47, 48]. The relative intensities for peaks of both the Ag3d_{5/2} and Mo3d_{5/2} remain unchanged over the whole composition range.

Figure-3 shows deconvoluted O1s spectrum for representative samples from region-I and region-II with composition (AgI)_{47.5}-(Ag₂O)₂₅-(MoO₃)_{26.25} and (AgI)_{42.5}-(Ag₂O)₂₅-(MoO₃)_{32.5} respectively. The O1s spectrum consists of the lattice oxygen (O_L) that is related to Ag-O bonding, adsorbed oxygen (O_A) that contains hydroxyl group, lattice defects and surface organic contaminations that result in C1s spectrum, oxygen bonded with Mo⁴⁺ (O_{Mo(IV)}) and Mo⁵⁺ (O_{Mo(V)}). The peak at 528.8 eV has been assigned to O_L, 530.7 eV to O_A [49], 531.7 eV to O_{Mo(IV)} [50] and 530.0 eV to O_{Mo(V)}.

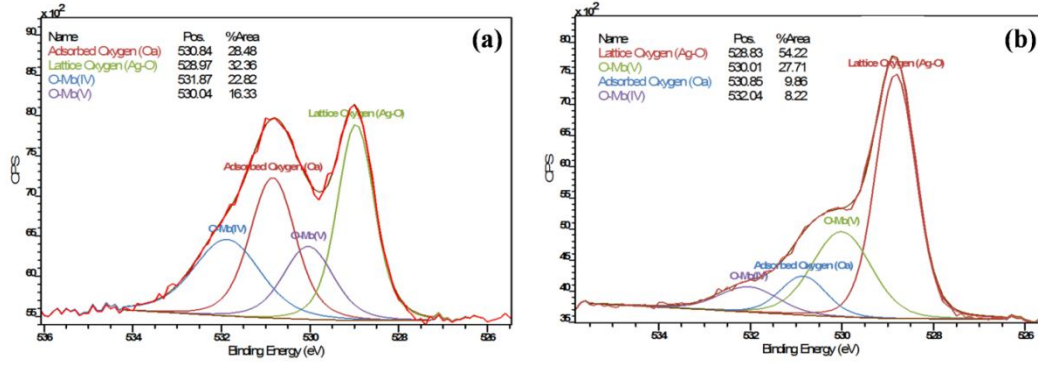


Figure-3: O1s spectrum for representative samples (a) $(\text{AgI})_{47.5}-(\text{Ag}_2\text{O})_{25}-(\text{MoO}_3)_{26.25}$ (b) $(\text{AgI})_{42.5}-(\text{Ag}_2\text{O})_{25}-(\text{MoO}_3)_{32.5}$

Figure-4 shows the change in relative intensities of all the oxygen peaks over the composition range. The relative intensity increases rapidly for O_L from region-I to region-II in expense of other oxygen species.

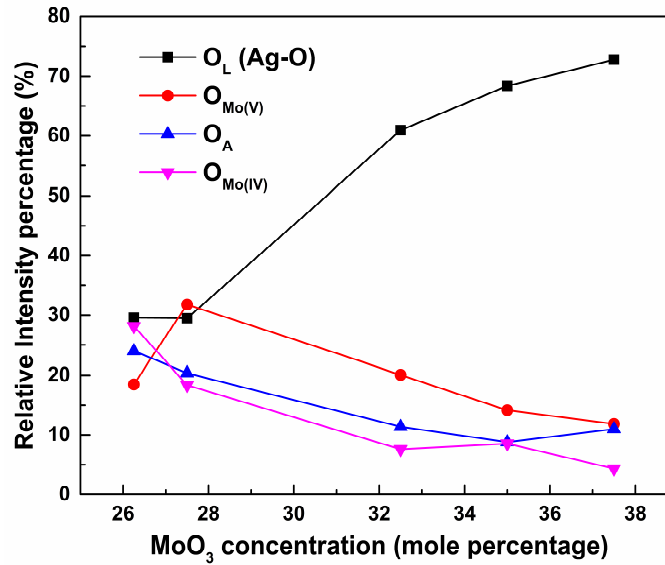
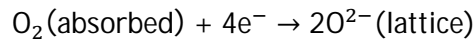


Figure-4: Relative intensities of oxygen species present in the sample

The O_A intensity decrement and its contribution to O_L intensity is interpreted by the equation



Part of these excess O_L populates around Ag while eventually increasing its oxidation state; this situation gets associated with the shift of Ag3d_{5/2} peak, a transition from Ag(I)-O in region-I to Ag(I, III)-O in region-II. O²⁻ is nucleophilic with a tendency to form metal-oxygen-metal bonds [50] and hence, part of O_L gets associated with less electronegative Mo and consequently modifies the O-Mo bonds. Both O_{Mo(IV)}

and $O_{Mo(V)}$ peaks shift towards lower binding energy (~ 0.21 eV for $O_{Mo(IV)}$ and ~ 0.51 eV for $O_{Mo(V)}$ with a significant decrease in relative intensity. Besides, Mo^{4+} and Mo^{5+} peak positions and intensity remain unchanged throughout the composition range. Thus, the oxidation of Ag and subsequent reduction of $O_{Mo(IV)}$ and $O_{Mo(V)}$ doesn't affect O_L and Mo species respectively. This situation suggests electron sharing and hence bond formation that can be interpreted as $[-Mo-O-Ag-O_L-]$. The oxidation states of Mo and O_L does not get affected at the expense of the formation of the (O-Ag) bond. $[-Mo-O-Ag-O_L-]$ is the structural unit of this glass that properly forms in region-II. These units are either absent or partially formed in region-I that might cause the clustering and hence negative heat capacity. Besides, the decrease in relative intensity of $O_{Mo(IV)}$ and $O_{Mo(V)}$ suggests that more Mo is being shared with less O that indicates formation of complex oxides of Mo. These conclusions together suggest an overall increase in covalent bonds and hence BO, during the transition from region-I to region-II. Previous discussion on negative heat capacity together with the present one concludes where and why the rigidity percolation should occur in this ion conducting conditional glass forming system.

Figure-5 shows the ΔH_{nr} profile over the whole composition range. The data acquisition technique has been rigorously discussed in earlier works by Micoulaut et al. [17]. The heat capacity study confirms the presence of NSPS within $20 \leq x \leq 30$ compositional range for samples $(AgI)_{75-x}-(Ag_2O)_{25}-(MoO_3)_x$. The gradual formation of $[-Mo-O-Ag-O_L-]$ bonds within the system incorporates with the decreasing profile of ΔH_{nr} with MoO_3 concentration, indicating a lowering value of ΔS_c . Beyond this threshold, the glassy system becomes necessarily and sufficiently covalent to exhibit the rigidity percolation phenomena.

The significance of the rigidity phases is well studied [8-14, 16-19]. In this work, we also pursue the same context of the significance. The FP is found to be within $31.25 \leq x \leq 32$ range. Beyond the FP, the system starts becoming rigid. The SRP appears to be in the range beyond $x \geq 35.5$. Between these two regions, within a range $32.25 \leq x \leq 35$, a square well like global minima appears, where the value of ΔH_{nr} becomes very less and hence $\Delta S_c \sim 0$. This phase happens to be mechanically rigid but stress free and known to be the IP. Thus, these results confirm the presence of rigidity percolation and NSPS in the ion conducting, conditional glass forming system, $(AgI)_{75-x}-(Ag_2O)_{25}-(MoO_3)_x$, which can be corroborated further with various distinct features of this system to improve the applicability and understanding.

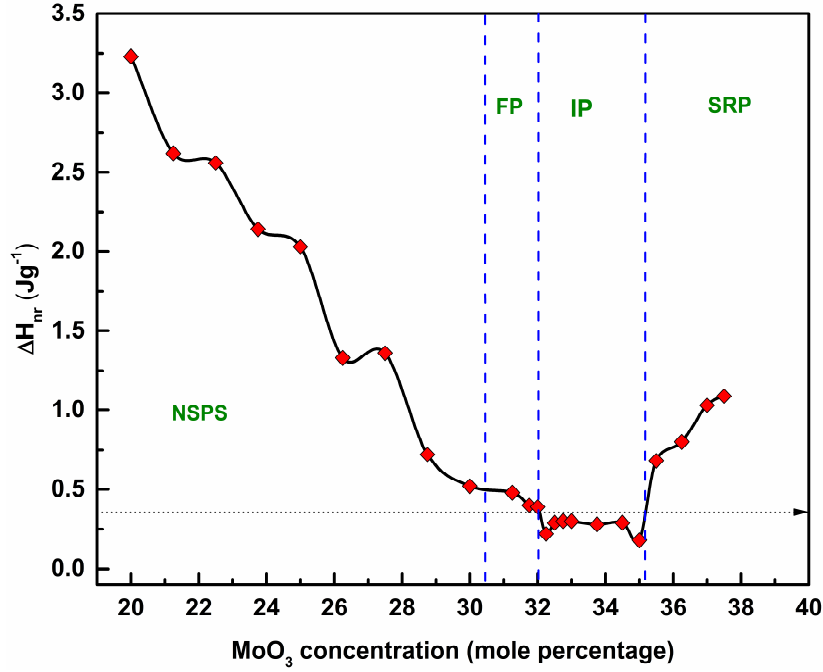


Figure-5: ΔH_{nr} (Jg⁻¹) vs. MoO₃ concentration (mole percentage)

In this work, we have investigated the rigidity percolation phenomena in a fast ion conducting, conditional glass forming system. The appearance of rigidity percolation in an ion conducting oxide glass system is not as apparent as in case of covalent chalcogen based glasses. The rigidity percolation fundamentally requires short range, nearest-neighbor covalent bonding where the first coordination number plays the most significant role; whereas in the case of long range, ionic bonding, and the percolation gets perturbed by higher order coordination. Besides, the glass formation in conditional glass formers is not smooth as for other excellent glass formers like SiO₂, GeO₂, P₂O₅ etc. There are significant differences between this conditional glass former and other glass formers from the chemical and topological aspects. The non-directional ionic bonds make the system fragile and the temperature dependence of viscosity deviates slightly from the Arrhenius behavior.

In order to know, at which threshold, this fluctuating behavior transforms into a stable profile, we thoroughly examined the nature of heat capacity. The absolute value of real, in phase, phase corrected reversing heat capacity changes sign, from negative to positive, during this transformation. The thermodynamic aspects of negative heat capacity suggest a heterogeneous clustering within the system. Earlier works on the pressure dependence of conductivity of AgI-Ag₂O-MoO₃ glass suggested a cluster model for this system and the studies on rigidity percolation on other oxide glass forming systems indicate that there is NSPS. In this work, based on the observation of sign change, we corroborate these two phenomena.

The XPS study reveals the formation of $[-\text{Mo}-\text{O}-\text{Ag}-\text{O}_\text{L}-]$ bonds to give rise to the required covalent nature within the system. These two conclusions together establish the reasonability of the existence of rigidity percolation of this glassy system. Finally, the measured value of ΔH_nr from ADSC experiment, while plotted against the composition range, exhibits a well like global minima within the range $32.25 \leq x \leq 35$. This denotes the IP where the system is rigid but stress free and the configurational entropy difference between solid and liquid becomes very less.

References

- ¹ W. Kauzmann, Chem. Rev. **43**, 219 (1948).
- ² J.C. Phillips, J. Non. Cryst. Solids **34**, 153 (1979).
- ³ M.F. Thorpe, J. Non. Cryst. Solids **57**, 355 (1983).
- ⁴ M.F. Thorpe, J. Non. Cryst. Solids **76**, 109 (1985).
- ⁵ J.C. Phillips and M.F. Thorpe, Solid State Commun. **53**, 699 (1985).
- ⁶ H. Hisakuni and K. Tanaka, Science (80-.). **270**, 974 (1995).
- ⁷ K.L. Chopra, K. Solomon Harshvardhan, S. Rajagopalan, and L.K. Malhotra, Solid State Commun. **40**, 387 (1981).
- ⁸ P. Boolchand, D.G. Georgiev, and B. Goodman, J. Optoelectron. Adv. Mater. **3**, 703 (2001).
- ⁹ P. Boolchand, G. Lucovsky, J.C. Phillips, and M.F. Thorpe, Philos. Mag. **85**, 3823 (2005).
- ¹⁰ X. Feng, W.J. Bresser, and P. Boolchand, Phys. Rev. Lett. **78**, 4422 (1997).
- ¹¹ D. Selvanathan, W.J. Bresser, P. Boolchand, and B. Goodman, Solid State Commun. **111**, 619 (1999).
- ¹² M. Micoulaut and M. Popescu, editors , *Rigidity and Boolchand Intermediate Phases in Nanomaterials*, 2009th ed. (INOE Publishing House, 2009).
- ¹³ A.J. Rader, B.M. Hespeneide, L.A. Kuhn, and M.F. Thorpe, Proc. Natl. Acad. Sci. **99**, 3540 (2002).
- ¹⁴ G. Lucovsky, D.A. Baker, M.A. Paesler, and J.C. Phillips, J. Non. Cryst. Solids **353**, 1713 (2007).
- ¹⁵ R. Zallen, *The Physics of Amorphous Solids* (Wiley Classic Library, Blacksburg, Virginia, 1998).

- ¹⁶ M. Micoulaut, M. Malki, D.I. Novita, and P. Boolchand, Phys. Rev. B **80**, 184205 (2009).
- ¹⁷ D.I. Novita, P. Boolchand, M. Malki, and M. Micoulaut, J. Phys. Condens. Matter **21**, 205106 (2009).
- ¹⁸ K. Rompicharla, D.I. Novita, P. Chen, P. Boolchand, M. Micoulaut, and W. Huff, J. Phys. Condens. Matter **20**, 202101 (2008).
- ¹⁹ Y. Vaills, T. Qu, M. Micoulaut, F. Chaimbault, and P. Boolchand, J. Phys. Condens. Matter **17**, 4889 (2005).
- ²⁰ K.J. Rao, *Structural Chemistry of Glasses*, First (Elsevier Ltd., Bangalore, India, 2002).
- ²¹ A. Jha, *Inorganic Glasses for Photonics: Fundamentals, Engineering and Applications* (John Wiley & Sons, Ltd, Leeds, UK, 2016).
- ²² T. Minami, T. Katsuda, and M. Tanaka, J. Non. Cryst. Solids **29**, 389 (1978).
- ²³ T. Minami and M. Tanaka, J. Non. Cryst. Solids **38 & 39**, 289 (1980).
- ²⁴ C.A. Angell, J. Non. Cryst. Solids **131–133**, 13 (1991).
- ²⁵ J. Swenson, R.L. McGreevy, L. Börjesson, J.D. Wicks, and W.S. Howells, J. Phys. Condens. Matter **8**, 3545 (1996).
- ²⁶ M. Tachez, R. Mercier, J.P. Malugani, and P. Chieux, Solid State Ionics **25**, 263 (1987).
- ²⁷ A. Fontana, F. Rocca, and M.P. Fontana, Phys. Rev. Lett. **58**, 503 (1987).
- ²⁸ B. Tanujit, G.S. Varma, and S. Asokan, (In Publ. (n.d.)).
- ²⁹ M. Reading and D. J. Hourston, editors , *Modulated-Temperature Differential Scanning Calorimetry: Theoretical and Practical Applications in Polymer Characterisation* (Springer, 2017).
- ³⁰ C.A. Angell, J. Non. Cryst. Solids **73**, 1 (1985).
- ³¹ R. Böhmer, K.L. Ngai, C.A. Angell, and D.J. Plazek, J. Chem. Phys. **99**, 4201 (1993).
- ³² J. Swenson and L. Börjesson, Phys. Rev. Lett. **77**, 3569 (1996).
- ³³ H. Senapati, G. Parthasarathy, S.T. Lakshmikumar, and K.J. Rao, Philos. Mag. B **47**, 291 (1983).
- ³⁴ K. Michaelian and I. Santamaría-Holek, Europhys. Lett. **79**, 43001 (2007).

- ³⁵ H.P. Cheng, X. Li, R.L. Whetten, and R.S. Berry, Phys. Rev. Lett. **65**, 1567 (1990).
- ³⁶ I. Santamaría-Holek and A. Pérez-Madrid, Phys. Rev. E **89**, 012144 (2014).
- ³⁷ M. Schmidt, R. Kusche, T. Hippler, J. Donges, W. Kronmüller, B. Von Issendorff, and H. Haberland, Phys. Rev. Lett. **86**, 1191 (2001).
- ³⁸ A. Aguado, Nat. Mater. **15**, 931 (2016).
- ³⁹ J.A. Reyes-Nava, I.L. Garzón, and K. Michaelian, Phys. Rev. B **67**, 165401 (2003).
- ⁴⁰ B. Cao, A.K. Starace, O.H. Judd, and M.F. Jarrold, J. Chem. Phys. **130**, 204303 (2009).
- ⁴¹ K. Gunasekera, S. Bhosle, P. Boolchand, M. Micoulaut, K. Gunasekera, S. Bhosle, P. Boolchand, and M. Micoulaut, J. Chem. Phys. **139**, 164511 (2013).
- ⁴² M. Mitkova and M.N. Kozicki, J. Phys. Chem. Solids **68**, 866 (2007).
- ⁴³ P. Boolchand, M. Jin, D.I. Novita, and S. Chakravarty, J. Raman Spectrosc. **38**, 660 (2007).
- ⁴⁴ P. Chen, C. Holbrook, P. Boolchand, D.G. Georgiev, K.A. Jackson, and M. Micoulaut, Phys. Rev. B **78**, 224208 (2008).
- ⁴⁵ G.B. Hoflund, Z.F. Hazos, and G.N. Salaita, Phys. Rev. B **62**, 11126 (2000).
- ⁴⁶ A. Adenier, M.C. Bernard, M.M. Chehimi, E. Cabet-Deliry, B. Desbat, O. Fagebaume, J. Pinson, and F. Podvorica, J. Am. Chem. Soc. **123**, 4541 (2001).
- ⁴⁷ J.G. Choi and L.T. Thompson, Appl. Surf. Sci. **93**, 143 (1996).
- ⁴⁸ P.A. Spevack and N.S. McIntyre, J. Phys. Chem. **96**, 9029 (1992).
- ⁴⁹ V. Kumar Kaushik, J. Electron Spectros. Relat. Phenomena **56**, 273 (1991).
- ⁵⁰ Y.C. Kang, R. Khanal, J.Y. Park, R.D. Ramsier, H. Khatri, and S. Marsillac, J. Vac. Sci. Technol. B **28**, 545 (2010).
- ⁵¹ J. L. G. Fierro, editor, *Metal Oxides: Chemistry and Applications* (Taylor & Francis, Berkeley, California, 2006).